Submitted to

Europhysics Conference on High Energy Physics, EPS2007, July 19-25, 2007, Manchester
Abstract: **178**
Parallel Session **Strong Interactions**

Electronic Access: www-h1.desy.de/h1/www/publications/conf/conf_list.html

Inelastic Electroproduction of Charmonium at HERA

H1 Collaboration

Abstract

Inelastic Electroproduction of J/ψ mesons is studied in ep-scattering at HERA. The data were taken with the H1 detector in the years 2004 to 2006 and correspond to an integrated luminosity of ~ 258 pb^{-1}. Single differential and double differential cross sections are measured with increased precision compared with previous analyses. The results are compared to theoretical predictions as implemented in Monte Carlo generators.

1 Introduction

Many models have been suggested to describe inelastic charmonium production in the framework of perturbative QCD, such as the color-singlet model (CSM) [1–4], the color-evaporation model [5, 6] and soft color interactions [7]. In the factorization ansatz of non-relativistic quantum chromodynamics (NRQCD) colour octet as well as colour singlet $c\bar{c}$ states contribute to the charmonium production cross section [8–10]. The size of these color octet contributions, described by long distance matrix elements (LDME), is defined by free parameters which have been determined in fits to the Tevatron data [11]. The NRQCD factorization approach contains the color singlet model which is recovered in the limit in which the color octet LDMEs tend to zero.

Calculations of cross sections for J/ψ production in deep-inelastic ep scattering at HERA have been performed in the NRQCD factorization approach at leading order in α_s taking into account diagrams of the type "$2 \rightarrow 2$" [12] using the matrix elements as determined in [11] and the MRST98LO [13] and CTEQ5L [14] parton distributions. In previous measurements [15–21] it was found that the calculations in the framework of NRQCD were not always capable of describing the data.

In this paper a measurement of J/ψ electroproduction is presented which provides improved statistical precision in comparison to the previous measurements. The data are compared with predictions from the event generators CASCADE [22] and EPJPSI [23]. Improved theoretical calculations in the framework of NRQCD are being performed [24] which should be tested with the new data.

2 H1 Detector

The H1 detector is described in detail in [25]. Charged particles emerging from the ep interaction region are measured by the central tracking detector (CTD) in the pseudo-rapidity range $-1.74 < \eta < 1.74$[1]. The CTD consists of two large cylindrical central jet drift chambers (CJCs) which are separated by a z-chamber and arranged concentrically around the beam-line in a magnetic field of 1.16 T. The CTD provides triggering information based on track segments from the CJC in the r-ϕ plane, transverse to the beam direction, and on the z-position of the vertex from the 5-layer multi-wire proportional chamber which is situated inside the inner CJC.

Charged and neutral particles are measured in the liquid argon (LAr) calorimeter, which surrounds the tracking chambers and covers the range $-1.5 < \eta < 3.4$, and in a lead–scintillating fibre calorimeter SpaCal, covering the backward region ($-4.0 < \eta < -1.4$) [26]. The measurements from the CTD and the calorimeters are combined to reconstruct the final state particles [27].

The calorimeters are surrounded by the solenoidal magnet and the iron return yoke which is instrumented with 16 layers of limited streamer tubes in the range $-2.5 < \eta < 3.4$, allowing the identification of muon tracks (CMD).

[1]The pseudo-rapidity is given by $\eta = -\ln\ \tan(\theta/2)$, where θ is measured with respect to the z-axis given by the proton beam direction.

The luminosity determination is based on the measurement of the Bethe-Heitler process ($ep \rightarrow ep\gamma$), where the photon is detected in a calorimeter located downstream of the interaction point in the electron beam direction[2].

3 Event Selection

The data sample corresponds to an integrated luminosity of $258\,\mathrm{pb}^{-1}$ and was recorded with the H1 experiment during the years 2004–2006. The events were triggered by a combination of signals from the calorimeters and the central drift chamber. Electroproduction events are selected by requiring that there be an isolated high energy electromagnetic cluster detected in the SpaCal consistent with a signal from the scattered electron. This restricts the range of negative four-momentum transfer squared to $3.6 < Q^2 < 100.$ GeV^2.

The J/ψ meson candidates are reconstructed through their decays into muons or electrons with branching ratio of $(5.93\pm0.06)\%$ and $(5.94\pm0.06)\%$, respectively [28]. Both lepton tracks are required to be of opposite charge, have a minimal transverse momentum of 800 MeV and fulfill the following lepton identification criteria: Decay electrons are identified via their energy deposition in the electromagnetic part of the calorimeter. Muon tracks are identified as minimum ionising particles in the LAr calorimeter or through track segments reconstructed in the CMD. Tracks from muon candidates are restricted to polar angles in the range $20^\circ < \theta < 160^\circ$ while electrons are selected in the range $30^\circ < \theta < 150^\circ$ in which the calorimeter identification is sufficiently controlled. To suppress contributions from elastic diffractive J/ψ production events are selected with a total of at least five reconstructed tracks beside the scattered electron in the central track detectors.

The number of signal events in each bin is determined by fits to the mass distributions in the interval $2 < m_{\ell\ell} < 6$ GeV. For both electron and muon samples the form of the fit to the signal, its width and position, is determined using data samples of elastic diffractive J/ψ mesons. These diffractive samples have large statistics with little background, thus allowing to determine the shape of the signals precisely. The signal in the muon sample is fitted by a Gaussian and the signal in the electron sample is fitted by a Gaussian with an additional exponential, describing the effect due to radiation of photons of the decay electrons. The background is parametrized by a polynomial of second order with three free parameters.

To correct for detector effects, such as detector resolutions and inefficiencies, large samples of signal events are generated using the Monte Carlo program CASCADE [22]. The results for CASCADE are cross checked using the J/ψ event generator EPJPSI [23]. All samples are passed through a detailed simulation of the H1 detector response based on the GEANT program [29] and the same reconstruction and analysis algorithms as used for the data.

The kinematics for charmonium production are described with the standard variables used for deep inelastic interactions, namely the square of the ep centre of mass energy, $s = (p+k)^2$, the squared four momentum transfer $Q^2 = -q^2$ and the mass of the hadronic final state $W = \sqrt{(p+q)^2}$. Here k, p and q are the four-momenta of the incident lepton, proton and virtual

[2]Between the beginning of 2005 and summer 2006 HERA was operated with electrons while in 2004 and after summer 2006 HERA was operated with positrons. In this paper we refer to the lepton beam as the electron beam.

photon, respectively. In addition, the scaled energy transfer $y = p \cdot q/p \cdot k$ (energy fraction transferred from the lepton to the hadronic final state in the proton rest frame) and the J/ψ fractional energy $z = (p_\psi \cdot p)/(q \cdot p)$ are used, where p_ψ denotes the J/ψ four-momentum.

The event kinematics are reconstructed using a method which combines the measurement of the scattered lepton and the hadronic final state to obtain good resolution in the entire kinematic range. The variable $Q^2 = 4\,E\,E' \cos^2 \frac{\theta_e}{2}$ is reconstructed from the energy E' and angle θ_e of the scattered lepton (E is the energy of the incoming lepton). For the calculation of y and z the hadronic final state is used in addition. Thus

$$y = \frac{\sum_{had}(E - p_z)}{\sum(E - p_z)} \qquad \text{and} \qquad z = \frac{p_\psi \cdot p}{y\,s/2} = \frac{(E - p_z)_\psi}{\sum_{had}(E - p_z)}, \tag{1}$$

where $\sum(E - p_z)$ runs over all the final state particles including the scattered lepton, and in $\sum_{had}(E - p_z)$ only the final state hadrons are summed. The J/ψ momentum is reconstructed from the momenta of the decay leptons. For the calculation of the sums in equations (1) a combination of tracks reconstructed in the CTD and energy depositions in the LAr and SpaCal calorimeters is used [27]. W is reconstructed using the relation $W^2 = ys - Q^2$.

The measurement is performed in the kinematic range $3.6 < Q^2 < 100$ GeV^2, $50 < W_{\gamma p} < 225$ GeV, $0.3 < z < 0.9$ and $p^*_{t,\psi} > 1$ GeV, where $p^*_{t,\psi}$ denotes the transverse momentum squared of the J/ψ in the $\gamma^* p$ center-of-mass frame.

4 Theory Calculations

Both Monte Carlo generators implement the CSM in leading order. The Monte Carlo generator CASCADE [22] contains an implementation of the k_t factorization approach using the CCFM evolution equation [30]. In CASCADE the direct heavy quark production processes $\gamma g \to c\bar{c}$ and $b\bar{b}$ are implemented using off-shell matrix elements convoluted with k_t-unintegrated parton distributions in the proton. In CASCADE, higher order parton emissions based on the CCFM [30] evolution equations are matched to $\mathcal{O}(\alpha_s)$ matrix elements in which the incoming parton can be off-shell.

EPJPSI is based on the DGLAP evolution [31]. Collinear factorization of the parton density distributions and the hard matrix elements is assumed. In the DGLAP approximation the evolution from the partons density distributions leads to a strong ordering of radiated partons in transverse momentum k_t. In contrast to the standard version used previously [16], the full dependence of the matrix element on Q^2 has been implemented [32].

Diffractive production of J/ψ and $\psi(2S)$ mesons is simulated using DIFFVM [33] with parameters which have been tuned to HERA measurements.

5 Results

The production cross section is measured by correcting the observed number of events in the signal for detector efficiencies and acceptances and dividing by the integrated luminosity.

The total systematic uncertainty of the cross section measurements is determined to be 10% for the muon sample and 11% for the electron sample, equal for all bins of the measurement. The dominant contributions to the systematic error come from uncertainties in the determination of the number of signal events and in the acceptance corrections, which rely on assumptions on the decay angular distributions of the J/ψ into leptons.

Figure 1 shows the invariant mass spectra of the selected events. A clear J/ψ signal can be seen. The number of events in the decay channel into muons is significantly larger due to the wider allowed angular range and higher efficiency for the identification of the decay leptons.

Measured differential cross sections are determined separately for the decay channels into muons and into electrons, correcting for acceptances as well as reconstruction and identification efficiencies specific to the decay lepton. The cross sections are then combined by averaging. The measured cross sections are not corrected for contributions from events with J/ψ mesons that are produced in decays of B-Mesons, χ_c or $\psi(2S)$ mesons.

The fraction of events arising from diffractive $\psi(2S)$ meson production with subsequent decay of the $\psi(2S)$ into $J/\psi + X$ is estimated to be 1.5% in the total sample and about 5% in the highest z bin. The fraction of events arising from b quarks decaying into $J/\psi + X$ is estimated to be 3.6% in the total sample and about 20% in the lowest z bin.

Differential cross sections are measured as functions of the following variables: Q^2, $W_{\gamma p}$, z and $p_{t,\psi}^{*2}$. The measured differential cross sections are shown in fig. 2. Shape comparisons of the data are performed with predictions from the CASCADE generator (solid line) and EPJPSI (dashed line). The total cross sections of the Monte Carlo simulations are normalized to the total cross section of the measurement. CASCADE shows a reasonable description of the dependence of Q^2. It reveals a somewhat harder distribution in $p_{t,\psi}^{*2}$ than the data. In contrast EPJPSI has a much steeper distribution in Q^2 and in $p_{t,\psi}^{*2}$. Both programs predict a somewhat steeper distribution of the cross section in $W_{\gamma p}$.

The distributions in $p_{t,\psi}^{*2}$ and z are further investigated (figs 3 and 4) by dividing the sample into bins of z and $p_{t,\psi}^{*}$, respectively. Both programs succeed in describing the z distribution overall as well as in bins of $p_{t,\psi}^{*}$. At small values of z, the dependence on $p_{t,\psi}^{*2}$ is better described by CASCADE while EPJPSI is better at large values of z.

6 Conclusions

A measurement of inelastic J/ψ production is performed in the kinematic range $3.6 < Q^2 < 100$ GeV^2, $50 < W_{\gamma p} < 225$ GeV, $0.3 < z < 0.9$ and $p_{t,\psi}^{*} > 1$ GeV with improved statistics and systematics with respect to previous measurements. Differential and double differential cross sections are measured and compared with predictions from the Monte Carlo models CASCADE and EPJPSI which both implement the color singlet model in leading order. Neither of the generators can describe all aspects of the data. After applying overall normalization factors, $d\sigma/dQ^2$ is reasonably described in CASCADE, while $d\sigma/dp^{*2}_{t,\psi}$ is too hard. Both distributions are too steep in EPJPSI. The modelling of $W_{\gamma p}$ is somewhat too steep compared to the data, the description of $d\sigma/dz$ is quite good, overall as well as in bins of $p^{*}_{t,\psi}$. The hardening of the $p^{*2}_{t,\psi}$ distribution with increasing inelasticity z is reproduced by both generators.

Acknowledgements

We are grateful to the HERA machine group whose outstanding efforts have made this experiment possible. We thank the engineers and technicians for their work in constructing and maintaining the H1 detector, our funding agencies for financial support, the DESY technical staff for continual assistance and the DESY directorate for support and for the hospitality which they extend to the non-DESY members of the collaboration.

References

[1] E. L. Berger and D. L. Jones, Phys. Rev. D **23** (1981) 1521.

[2] R. Baier and R. Rückl, Nucl. Phys. B **201** (1982) 1.

[3] R. Baier and R. Rückl, Phys. Lett. B **102** (1981) 364.

[4] R. Baier and R. Rückl, Z. Phys. C **19** (1983) 251.

[5] F. Halzen, Phys. Lett. B **69** (1977) 105.

[6] O. J. P. Eboli, E. M. Gregores and F. Halzen, Phys. Lett. B **451** (1999) 241 [hep-ph/9802421].

[7] A. Edin, G. Ingelman and J. Rathsman, Phys. Rev. D **56** (1997) 7317 [hep-ph/9705311].

[8] W. E. Caswell and G. P. Lepage, Phys. Lett. B **167** (1986) 437.

[9] B. A. Thacker and G. P. Lepage, Phys. Rev. D **43** (1991) 196.

[10] G. T. Bodwin, E. Braaten and G. P. Lepage, Phys. Rev. D **51** (1995) 1125 [Erratum-ibid. D **55** (1997) 5853] [hep-ph/9407339].

[11] E. Braaten, B. A. Kniehl and J. Lee, Phys. Rev. D **62** (2000) 094005 [hep-ph/9911436].

[12] B. A. Kniehl and L. Zwirner, Nucl. Phys. B **621** (2002) 337 [hep-ph/0112199].

[13] A.D. Martin, R.G. Roberts, W.J. Stirling and R.S. Thorne, Eur. Phys. J. **C4**, 463 (1998) hep-ph/9803445.

[14] H.L. Lai *et al.* [CTEQ Collaboration], hep-ph/9903282.

[15] S. Aid *et al.* [H1 Collaboration], Nucl. Phys. B **472** (1996) 3 [hep-ex/9603005].

[16] C. Adloff *et al.* [H1 Collaboration], Eur. Phys. J. C **10** (1999) 373 [hep-ex/9903008].

[17] C. Adloff *et al.* [H1 Collaboration], Eur. Phys. J. C **25** (2002) 25 [hep-ex/0205064].

[18] C. Adloff *et al.* [H1 Collaboration], Eur. Phys. J. C **25** (2002) 41 [hep-ex/0205065].

[19] J. Breitweg *et al.* [ZEUS Collaboration], Z. Phys. C **76** (1997) 599 [hep-ex/9708010].

[20] S. Chekanov *et al.* [ZEUS Collaboration], Eur. Phys. J. C **27** (2003) 173 [hep-ex/0211011].

[21] S. Chekanov *et al.* [ZEUS Collaboration], hep-ex/0505008.

[22] H. Jung and G.P. Salam, Eur. Phys. J. C **19** (2001) 351 [hep-ph/0012143];
H. Jung, Comput. Phys. Commun. **143** (2002) 100 [hep-ph/0109102].

[23] H. Jung, in: Proc. of the Workshop on Physics at HERA, ed. W. Buchmüller and G. Ingelman, Hamburg (1992), Vol. 3, p. 1488;
H. Jung, D. Krücker, C. Greub and D. Wyler, Z. Phys. C **60** (1993) 721.

[24] B.A. Kniehl, Private Communication.

[25] I. Abt *et al.* [H1 Collaboration], Nucl. Instrum. Meth. A **386** (1997) 310 and 348.

[26] T. Nicholls *et al.* [H1 SPACAL Group Collaboration], Nucl. Instrum. Meth. A **374** (1996) 149.

[27] M. Peez, PhD Thesis, Univ. Lyon, 2003, available at http://www-h1.desy.de/publications/theses.list.html.

[28] W.-M. Yao *et al.* [Particle Data Group] J. Phys. G 33, 1 (2006).

[29] R. Brun *et al.*, CERN-DD/EE-84-1 (1987).

[30] M. Ciafaloni, Nucl. Phys. B **296** (1988) 49; S. Catani, F. Fiorani and G. Marchesini, Phys. Lett. B **234** (1990) 339; *idem*, Nucl. Phys. B **336** (1990) 18; G. Marchesini, Nucl. Phys. B **445** (1995) 49.

[31] V.N. Gribov and L.N. Lipatov, Yad. Fiz. **15** (1972) 781 [Sov. J. Nucl. Phys. **15** (1972) 438]; G. Altarelli and G. Parisi, Nucl. Phys. B **126** (1977) 298; Y.L. Dokshitzer, Sov. Phys. JETP **46** (1977) 641 [Zh. Eksp. Teor. Fiz. **73** (1977) 1216].

[32] K. Krüger and S. Mohrdieck, in: Proc. of the Workshop on Monte Carlo generators for HERA physics, ed. A. T. Doyle *et al.,* DESY-PROC-1999-02 (1999) 497; D. Krücker, "Models for Inelastic J/ψ Production at HERA", PhD thesis (1995) RWTH Aachen (in German, http://www-h1.desy.de/publications/theses_list.html).

[33] B. List and A. Mastroberardino, in: Proc. of the Workshop on Monte Carlo generators for HERA physics, ed. A. T. Doyle *et al.,* DESY-PROC-1999-02 (1999) 396.

[34] M. Beneke, M. Krämer and M. Vanttinen, Phys. Rev. D **57** (1998) 4258 [hep-ph/9709376].

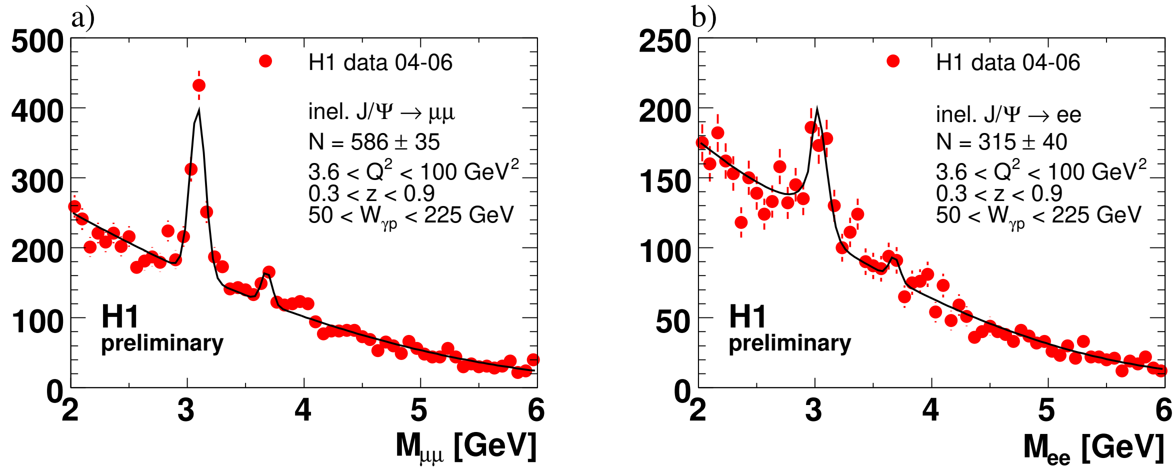

Figure 1: Invariant mass spectrum of a) two oppositely charged muons and b) two oppositely charged electrons. All selection cuts are applied. The line shows the result of a fit to signal and background.

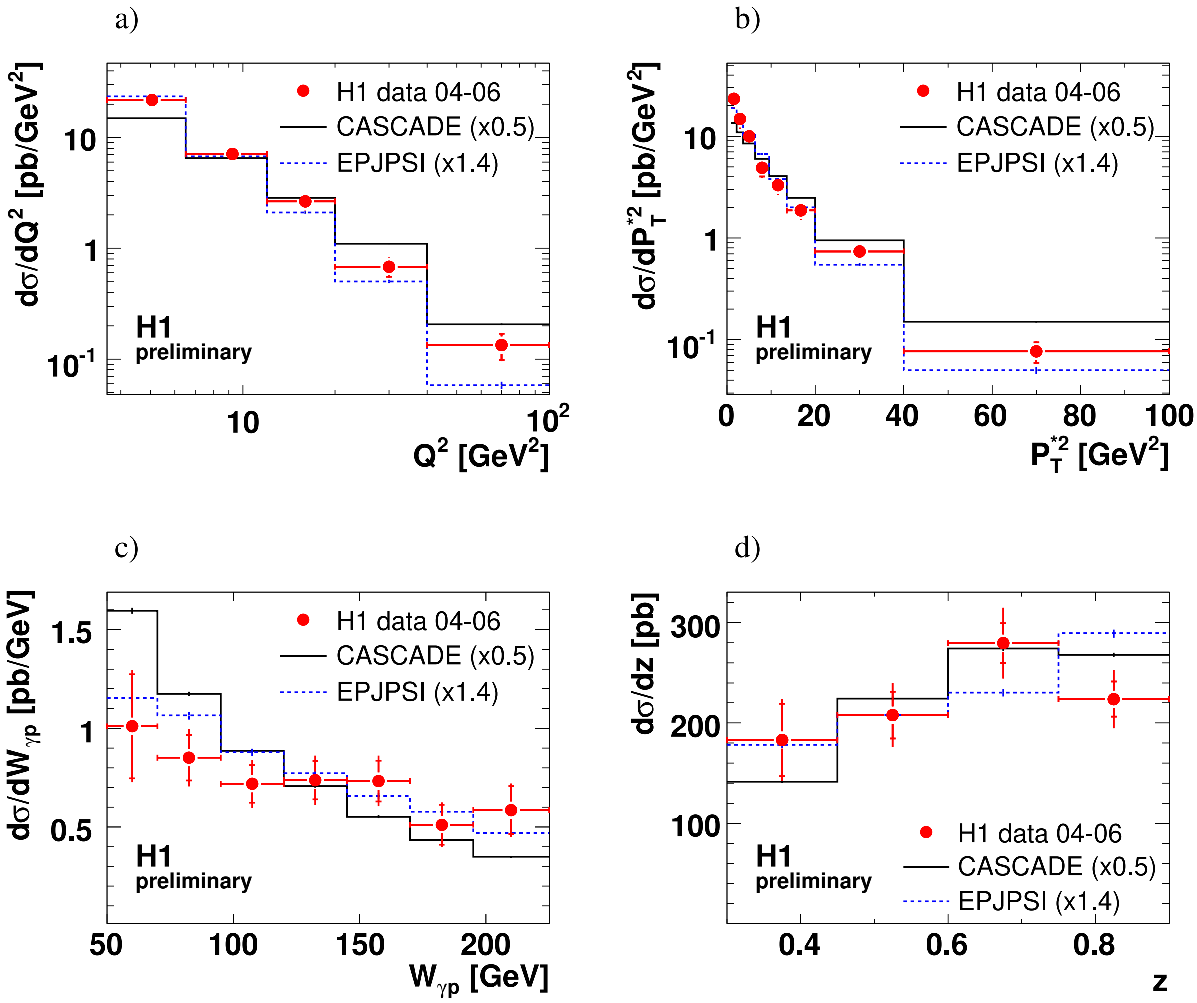

Figure 2: Differential J/ψ cross sections for the kinematic range $Q^2 > 3.6$ GeV^2, $50 < W_{\gamma p} < 225$ GeV, $0.3 < z < 0.9$ and $p_{t,\psi}^{*2} > 1$ GeV, as functions of a) Q^2, b) $p_{t,\psi}^{*2}$, c) $W_{\gamma p}$, d) z. The data are compared to the predictions from CASCADE (solid line) and EPJPSI (dashed line).

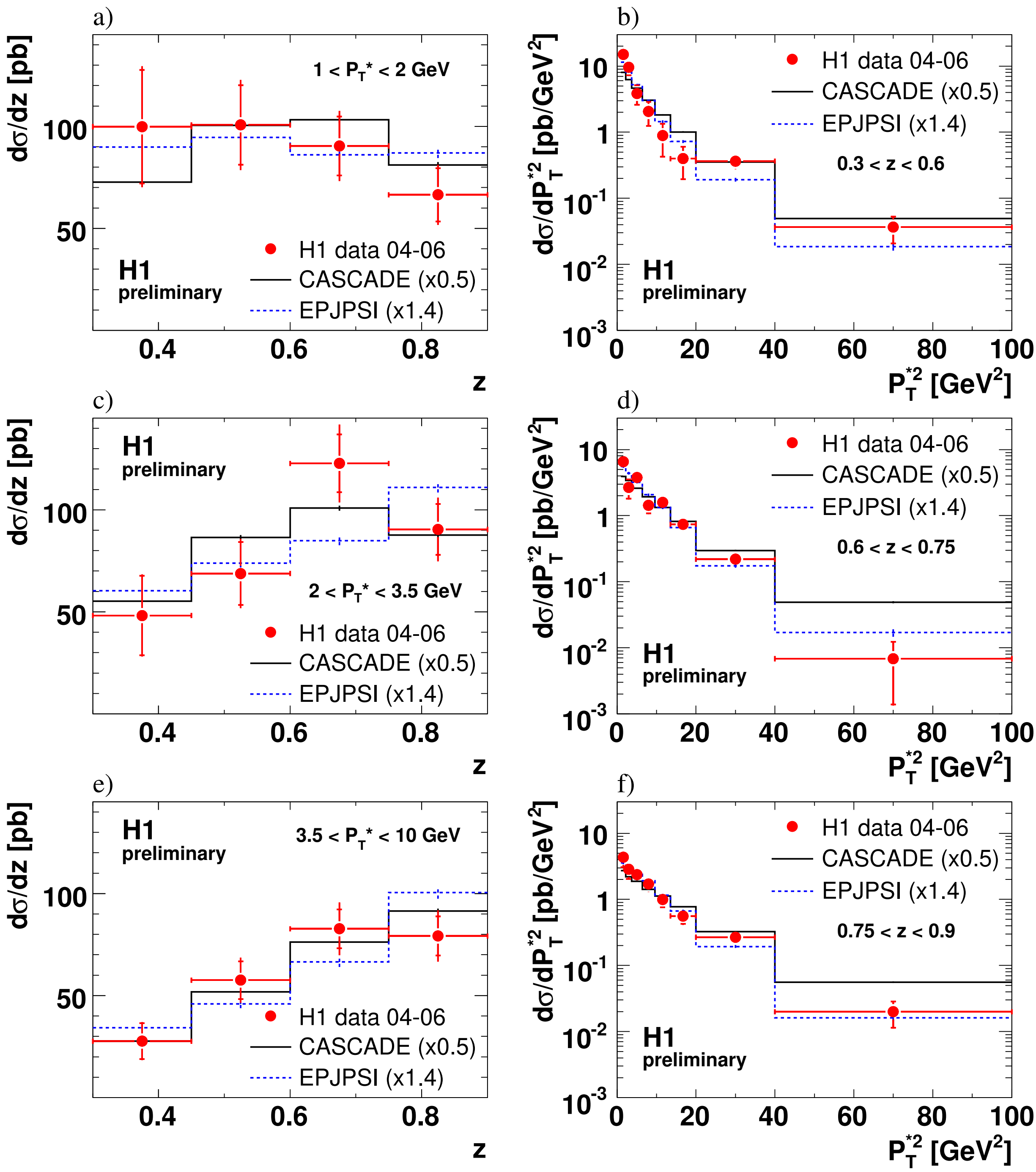

Figure 3: Differential J/ψ cross sections, $d\sigma/dz$ as a function of z in three bins of $p^*_{t,\psi}$, a) $1 < p^*_{t,\psi} < 2$ GeV, c) $2 < p^*_{t,\psi} < 3.5$ GeV, e) $3.5 < p^*_{t,\psi} < 10$ GeV and $d\sigma/dp^{*2}_{t,\psi}$ as a function of $p^{*2}_{t,\psi}$ in three bins of z, b) $0.3 < z < 0.6$, d) $0.6 < z < 0.75$ and f) $0.75 < z < 0.9$. The predictions from CASCADE (solid line) and EPJPSI (dashed line) are also shown.

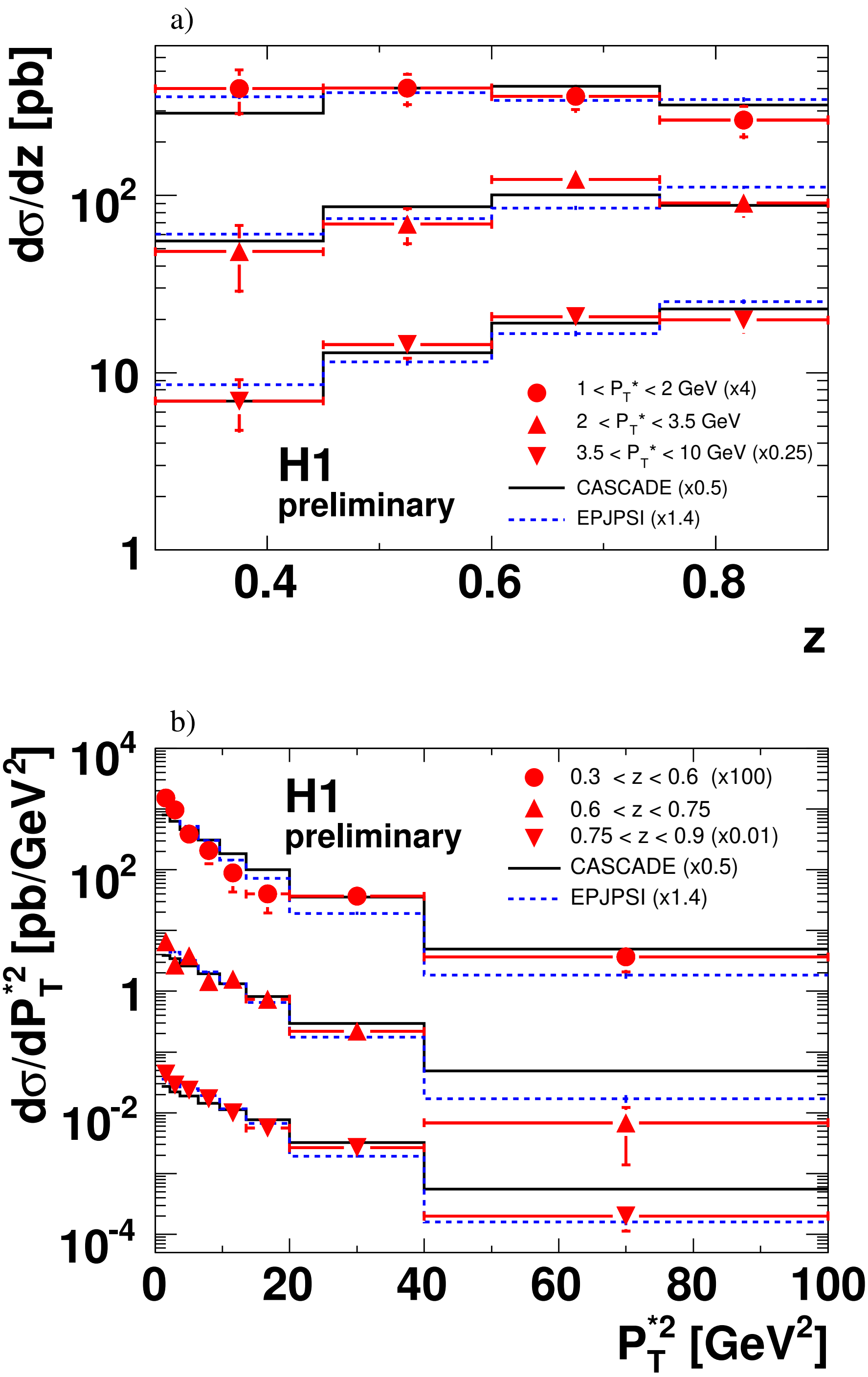

Figure 4: Differential J/ψ cross sections, $d\sigma/dz$ as a function of a) z in three bins of $p^*_{t,\psi}$, $1 < p^*_{t,\psi} < 2$ GeV, $2 < p^*_{t,\psi} < 3.5$ GeV, $3.5 < p^*_{t,\psi} < 10$ GeV and b) $d\sigma/dp^{*2}_{t,\psi}$ as a function of $p^{*2}_{t,\psi}$ in three bins of z, $0.3 < z < 0.6$, $0.6 < z < 0.75$ and $0.75 < z < 0.9$. The predictions from CASCADE (solid line) and EPJPSI (dashed line) are also shown.